Research Article

Micol Palmieri, Ilaria Giannetti, and Andrea Micheletti*

Floating-bending tensile-integrity structures**

https://doi.org/10.1515/cls-2021-0008
Received Oct 09, 2020; accepted Jan 24, 2021

Abstract: This is a conceptual work about the form-finding of a hybrid tensegrity structure. The structure was obtained from the combination of arch-supported membrane systems and diamond-type tensegrity systems. By combining these two types of structures, the resulting system features the "tensile-integrity" property of cables and membrane together with what we call "floating-bending" of the arches, a term which is intended to recall the words "floating-compression" introduced by Kenneth Snelson, the father of tensegrities. Two approaches in the form-finding calculations were followed, the Matlab implementation of a simple model comprising standard constant-stress membrane/cable elements together with the so-called stick-and-spring elements for the arches, and the analysis with the commercial software WinTess, used in conjunction with Rhino and Grasshopper. The case study of a T3 floating-bending tensile-integrity structure was explored, a structure that features a much larger enclosed volume in comparison to conventional tensegrity prisms. The structural design of an outdoor pavilion of 6 m in height was carried out considering ultimate and service limit states. This study shows that floating-bending structures are feasible, opening the way to the introduction of suitable analysis and optimization procedures for this type of structures.

Keywords: conceptual design; tensile integrity; floating bending; temporary structure; deployable structure

1 Introduction

This paper focuses on a conceptual work about the form-finding of a hybrid tensegrity structure. Hybrid tensegrity systems have been considered several times in the literature with noteworthy studies, such as, the cocoon method by Sakantamis and Popovic Larsen [1], the tensegrity-membrane structure obtained numerically by Shigematsu, Tanaka, and Noguchi in 2008 [2], and the *tensairity* concept proposed by Luchsinger, Pedretti, and Reinhard in 2004 [3].

The present hybrid tensegrity structure was obtained from the combination of arch-supported membrane systems and diamond-type tensegrity systems. As shown in Figure 1, the diamond pattern highlighted in the tensegrity module, recalls the shape of a simple arch-supported membrane.

In the first attempt to combine these two structures, the classic triangular tensegrity prism, or T3, "patched" with three arch-supported membranes, was considered. Figure 2 shows the transformation process and, in the last image, the resulting system, in which three arches are suspended against each other by membranes and cables, forming a free-standing system. The obtained structure was shaped as

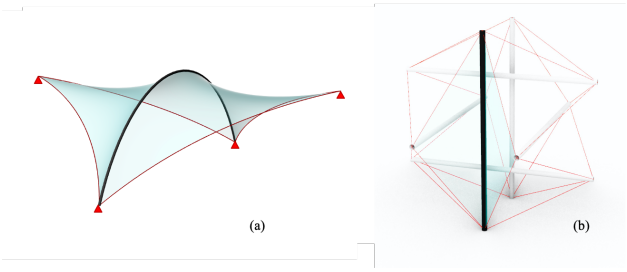

Figure 1: An arch-supported membrane structure (left) and a diamond-type tensegrity system (right).

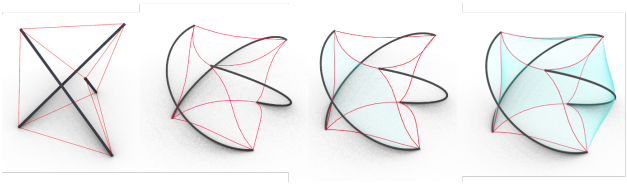

Figure 2: From left to right, successive conceptual transformations of a T3 tensegrity module resulting in a structure with floating arches, cables, and membrane.

***Corresponding Author: Andrea Micheletti:** Department of Civil and Computer Science Engineering, University of Rome 'Tor Vergata', Italy; Email: micheletti@ing.uniroma2.it
Micol Palmieri, Ilaria Giannetti: Department of Civil and Computer Science Engineering, University of Rome 'Tor Vergata', Italy
** Paper included in the Special Issue entitled: Shell and Spatial Structures: Between New Developments and Historical Aspects

a continuous surface with two types of singularities, which correspond to the curves occupied by cables and arches. This new system features the "tensile-integrity" of cables and membrane, together with what we called "floating-bending" of the arches, a term which is intended to recall the words "floating-compression", often mentioned by Kenneth Snelson, the father of tensegrities, to refer to the constructions he realized [4]. It is worth observing that the arches are subjected to shear and torsion, in addition to compression and bending. Moreover, arches are not active-bending, *i.e.*, their configuration at rest is curved and undergoes small deformations at the prestressed equilibrium state.

In the form-finding calculations two approaches were followed. The first one is the implementation in Matlab of a simple model comprising standard constant-stress membrane and cable elements, and the so-called *stick-and-spring* elements for the arches. The model refers to Arcaro's implementation for the membrane elements [5], and to Favata, Micheletti, Podio-Guidugli, Pugno [6] for the implementation of stick-and-spring elements. The second approach followed in the form-finding calculations is that of performing the analyses with the commercial software WinTess [7, 8], used in conjunction with Rhino and Grasshopper to obtain a parametric mesh of the structure. The structural design of an outdoor pavilion of 6 m in height was carried out considering ultimate and service limit states.

Similarly to the case of conventional tensegrity systems, possible applications could regard deployable and temporary structures, with the advantage of having a much larger enclosed volume, without having the struts placed internally to the convex hull of the system, as in the case of the traditional tensegrity prism (Figure 3). This study shows that floating-bending structures are feasible, and that they may provide interesting architectural and engineering solutions, opening the way to the introduction of suitable analysis and optimization procedures for this type of structures.

The paper is organized as follows. In Section 2, the Matlab implementation of the simple membrane/stick-and-spring model is briefly presented, together with the form-finding results obtained by minimization of the total potential energy. Section 3 describes the form-finding analysis and the structural design performed with WinTess, with reference to the case of an outdoor pavilion. A discussion of results and possible design possibilities follows in Section 4, while our conclusions are given in Section 5.

2 Membrane and stick-and-spring elements for form-finding

A simple model for form-finding is described in this section. An equilibrium configuration for the modified T3 module was found by minimizing the total elastic energy considering linearly elastic elements in a large displacement regime. Calculations were carried out using Matlab. Membrane elements were implemented following [5], while stick-and-spring elements following [6].

More specifically, the structural model is given by the quintuplet S = (N,E,W,Z,M), consisting of: (i) a set N of points, called *nodes*, of the Euclidean space; (ii) a collection E of *edges*, *i.e.*, two-elements subset of N; (iii) a collection W of *wedges*, *i.e.*, three-elements subsets of N, (iv) a collection Z of z-edges, *i.e.*, four-elements subsets of N; (v) a collection M of triangular membrane elements, identified by three-element subsets of N. The edges connecting nodes $i, j \in N$ is denoted by $ij \in E$ and has length l_{ij}. We say that $ijk \in W$, with $i, j, k \in N$, is the wedge that has *head node i* and *tail nodes j* and k, with ϑ_{ijk} the angle $\angle jik$, while $ijkh \in Z$ is the z-edge on the chain of four nodes $i, j, k, h \in N$, with Θ_{ijkh} the dihedral angle between the two planes containing *i,j,k* and *j,k,h* respectively. Furthermore, a membrane element $m \in M$ has volume v_m, constant elasticity tensor C_m, and vector of strain components ϵ_m, uniform on the element and depending only on its nodal positions, as defined in [5]. In the stick-and-spring model each arch is composed of bars hinged together, with rotational elastic springs which respond to bending and torsion deformations of the arch, as shown in Figure 4.

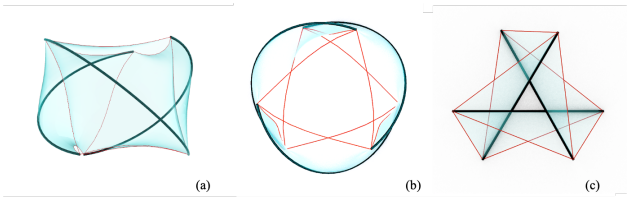

Figure 3: Side (a) and top view (b) of the modified T3. Top view of the classical T3 (c).

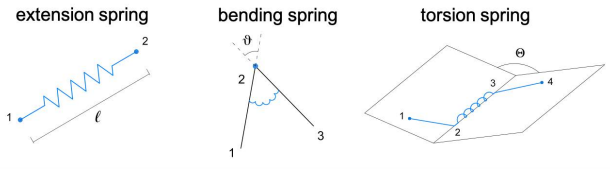

Figure 4: The three types of spring elements considered to model the arches in the stick-and-spring model, associated to edges, wedges, and z-edges.

The elastic energy Π of the system S has five contributions: the energy of triangular, uniform stress/uniform strain, membrane elements, composing the membrane patches; the energy of bar, axial-only, elements for cables; the energy of the three types of spring elements attached to the arches, accounting for their extension, bending, and torsion deformations. The elastic energy is then given by the following expression

$$
\begin{aligned}
2\Pi(p) = & \sum_{m\in M} v_m C_m \epsilon_m(p)\cdot\epsilon_m(p) + \sum_{ij\in E}\kappa_{ij}\left(l_{ij}(p)-l_{0ij}\right)^2 \\
& + \sum_{ijk\in W}\lambda_{ijk}\left(\vartheta_{ijk}(p)-\vartheta_{0ijk}\right)^2 \\
& + \sum_{ijkh\in Z}\mu_{ijhk}\left(\Theta_{ijkh}(p)-\Theta_{0ijkh}\right)^2,
\end{aligned}
$$

where p denotes the vector containing all the nodal position vectors, κ_{ij}, λ_{ijk}, μ_{ijhk} denote the spring constants of edges, wedges and z-edges respectively, and l_{0ij}, ϑ_{0ijk}, Θ_{0ijkh} denotes the values at rest of the edge length, and the angles of wedges and z-edges respectively. Edges with different properties account for the two types of contributions of cables and extension spring, which are both included in the second summation in the expression above. The current length of edge ij is $l_{ij} = |p_i - p_j|$, with p_i, p_j the position vectors of i and j. On denoting by $n_{ij} = (p_j - p_i)/l_{ij}$ the unit vector pointing from node i to node j, the current wedge angle is determined by the relation $|n_{ij}||n_{ik}|\cos\vartheta_{ijk} = (n_{ij}\cdot n_{ik})$. On denoting the unit normal to the plane containing nodes i,j,k, by $m_{ijk} = (n_{ij}\times n_{jk})/|n_{ij}\times n_{jk}|$, the current z-edge angle is determined by the relation $|m_{ijk}||m_{jkh}|\cos\Theta_{ijkh} = (m_{ijk}\cdot m_{jkh})$.

The form-finding problem for a cantilevered arch was first considered as prototypical example, obtaining an arch-supported membrane pinned to ground at just three points, as shown in Figure 5(a). Matlab calculations were then performed for the modified T3 prism. Starting from the classical T3 configuration, struts were replaced with arches, and the equilibrium configuration of membrane patches was found considering them attached to the arch and bounding cables fixed in space. Afterward, the constraints fixing arches and cables were eliminated, leaving just six scalar constraints to block rigid-body motions, and the form-finding process was repeated.

In each of these form-finding problems, the value of spring constants of edges, wedges, and z-edges forming the arches was taken numerically much larger than the elastic constants of membrane and cables, so that the equilibrium shape of the arches remains close to the initial one. The values of length and area at rest, respectively for cables and membrane elements, were assigned suitably smaller than those at equilibrium, while the spring elements for the arches were considered at rest in the initial configuration.

It is worth noticing that these quantities, together with all the elastic constants, are virtual quantities which do not need to correspond to any preliminary choice of materials. In particular, the spring constants were assigned arbitrarily, and they were not obtained as lumped values of an equivalent continuum. We are only interested in finding one configuration where internal forces are in equilibrium, assuming that such equilibrium forces can be successively matched and assigned to different values of spring constants and rest lengths/areas.

As all the elements' strain measures are expressed as functions of nodal positions, these were taken as free variables and the built-in Matlab function *fminunc* was used to perform the minimization procedure. Figure 5(b) shows an image of the equilibrium configuration found. It can be noticed, by looking at the elastic energy of the membrane, Figure 5(c), that the ridge cables redistribute and balance the stress difference on the two adjacent membrane patches.

Lastly, the equilibrium solution resulting from Matlab computations was checked with the *Analysis* module of the WinTess software by assigning a negligible self-weight to all elements, a 2% prestrain to the membrane, rest lengths equal to the equilibrium lengths computed in Matlab to cables and arches, and by choosing cross-sectional dimensions customarily. WinTess iterative calculations led to a slightly different equilibrium configuration in a few iterations (Figure 5d), thus providing a qualitative confirmation

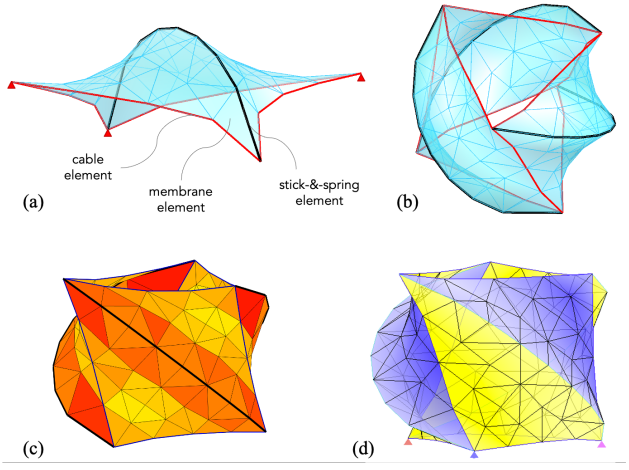

Figure 5: Matlab implementation: model of the cantilevered arch (a); equilibrium configuration of the modified T3 module (b); colormap of the elastic energy of the membrane, higher values at darker colors (c). WinTess check: equilibrium configuration of the same system as obtained in WinTess (d).

of the form found. We refer the reader to the next section for more details on the WinTess calculation procedure.

3 Case study: form-finding and structural design of a floating-bending pavilion

In this section, the case study of a modified T3 composed by steel tubes arches, steel cables and a polyester membrane is presented. The prism has height equal to 6 m and triangular base inscribed in a circle of 7.7 m in diameter, while the arches span a length of 9.6 m with a rise of 2.8 m. Two distinct versions of the structure were considered: the *closed* version, analogous to the system described in the previous section, a modified T3 with three-fold cyclic-symmetry; the *open* version, where one of the patches was replaced by tension ties in order to obtain a lateral opening to access the space inside the structure (Figure 6).

The following design flow was adopted. A parametric geometric model of the T3 tensegrity prism, with membrane and curved beams, was obtained by using the Grasshopper code in Rhinoceros. The membrane was described as a piece-wise conical continuous surface (Figure 6a), containing the edge cables of the T3 and the three arches. The Delaunay triangulation algorithm available in Grasshopper was used to generate a mesh, starting from a regular grid of points on the surface. Such mesh was then refined with a chosen pattern of elements of equal area. The mesh obtained in this way can be imported in the WinTess software (Figure 6a, 6b) to perform the form-finding analysis, using the force-density method. The mesh was transformed in a finite-element model of the structure by taking advantage of the WinTess interface.

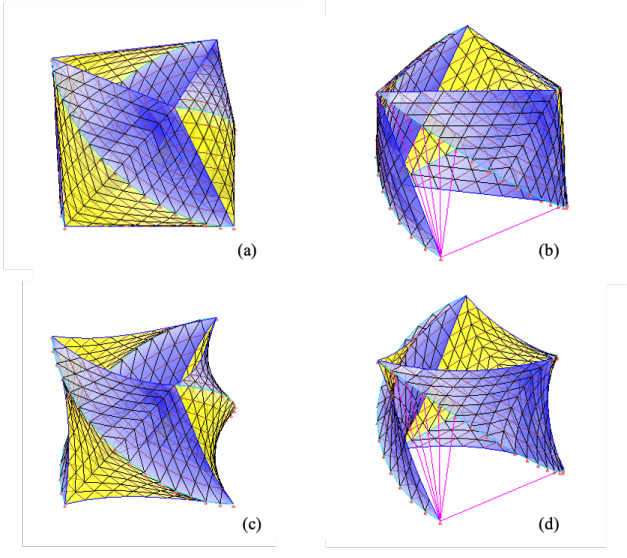

Figure 6: Snapshot of the WinTess model before form-finding (a, b) and after form-finding (c, d) for the closed and open version of the structure.

In both the closed and the open versions, the WinTess *Form-finding* module was run choosing a ratio between the force-densities of membrane and cables assigned equal to 1/10. In this phase, all nodes on the arches were constrained to the ground, because the force-density-based Form-finding module of WinTess does not allow to find the equilibrium configuration of beams and arches, while this is possible in the large-displacement iterative procedure which was performed in the Analysis module of the software. The configurations resulting from the WinTess form-finding calculation are shown in Figure 6(c, d). The form-finding procedure of the present structure was completed in the Analysis module of WinTess, where constraints on the arches were released, actual material properties were assigned to all elements, and nonlinear iterative calculations were performed to find the equilibrium configuration under self-weight and prestress.

The modified T3 module was dimensioned and verified under snow and wind loads, under ultimate limit states (ULS) considering a wind reference speed of 97.2 km/h, a snow load of 0.48 kN/m^2, and the ULS coefficients shown in Table 1. This process led to the choice of materials and sections shown in Table 2. The ratio between actual stress and allowable stress for ULS in each element remains below 0.65 for cables and membrane, and below 0.86 for the tubular arches. Figure 7 (left) shows a diagram of the bending moments of the arches, in kNm, together with the values of the axial forces, in kN, of cables and arches for the open structure. Maximum values of internal actions for the case of ULS under self-weight and prestress, with and without wind load are reported in Table 3. Bending moments of the arches, and axial forces of cables and arches at the ULS equilibrium configuration under self-weight, prestress, and

Table 1: ULS coefficients used in the analysis.

ULS coefficients			
loads		materials	
self weight	1.3	membrane	3
wind	1.5	cables	1.67
snow	1.5	tubes	1.65
internal pressure	1		
prestress	1.1		

Table 2: Materials and section of the elements of the structure.

membrane	elastic modulus	strength
Ferrari Fluotop T2 702 (PVC)	400 kN/m	300/280 daN/5cm
cables	diameter	strength
6×19 fibre core galvanized steel wire rope	16 mm	
arches	diameter	thickness
S430 steel circular tube	320 mm	20 mm

Table 3: Maximum values of internal actions for the ULS, for both the closed structure and the open structure, considering prestress (PS) and self-weight (SW), with and without wind load (W).

		closed structure		open structure	
		PS+SW	PS+SW+W	PS+SW	PS+SW+W
membrane					
membrane stress	(kN/m)	6.605	12.832	6.244	12.787
cables					
axial force	(kN)	27.635	56.000	27.754	65.553
arches					
axial force	(kN)	−69.859	−120.07	−69.366	−113.661
bending moment	(kN m)	248.09	401.213	250.156	415.957
shear force	(kN)	59.475	92.264	63.642	106.985
torsion moment	(kN m)	2.534	4.023	2.547	6.948

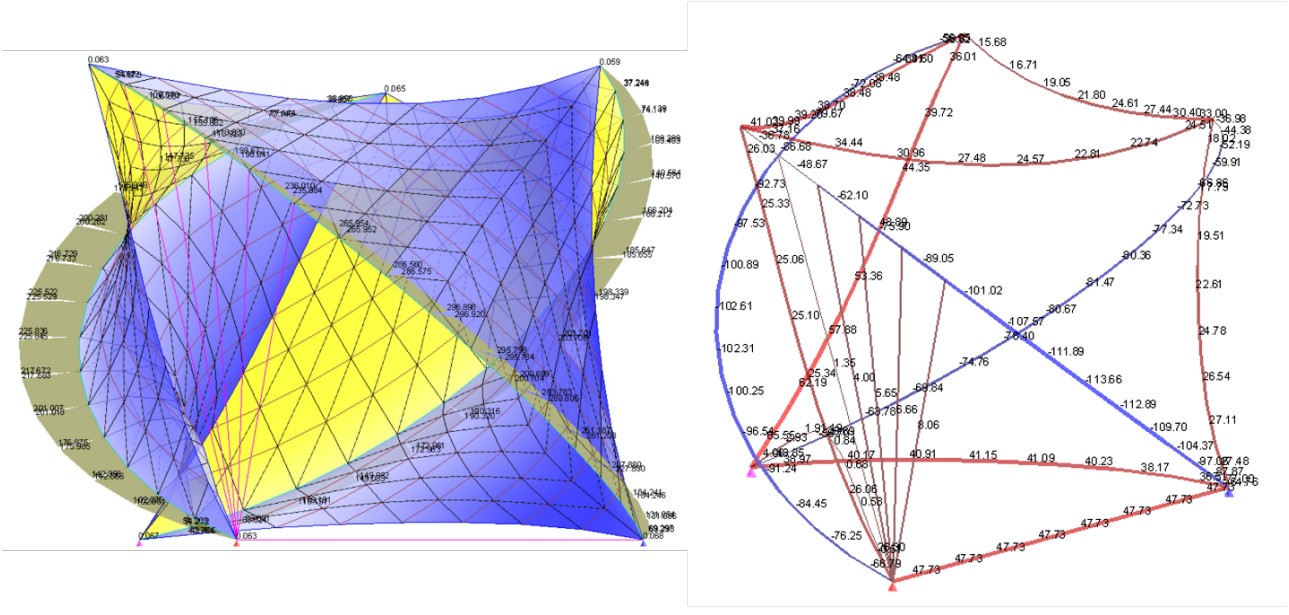

Figure 7: Bending moments of the arches, in kNm (left) and axial forces of cables and arches, in kN (right), at the equilibrium configuration under ULS with self-weight, prestress, and wind load.

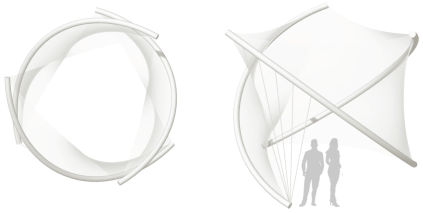

Figure 8: Artistic impression of the designed pavilion, top view and side view.

wind load are shown in Figure 7. An artistic impression of the final design is depicted in Figure 8.

4 Design of floating-bending structures

The floating-bending concept can be applied to many diamond-type modules with different number of bars [9]. The simplest system of this kind we can think of is the one obtained by modifying the T2, also called tensegrity kite. The modified T2 module is shown in Figure 9(a, b), and it resembles a sort of prestressed pillowcase. Figure 9(c, d, e) shows a five-bar tensegrity module and two views of its modified floating-bending version.

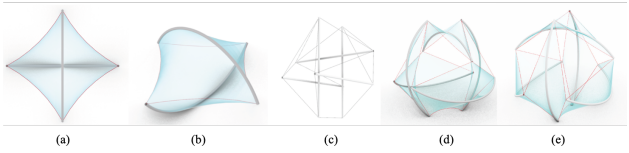

Figure 9: Floating-bending concept applied to different diamond-type modules with different number of bars [9].

Other more elaborate examples can be found by looking at Fuller's balloon analogy, which recognizes how stable tensegrity systems have compression inside and tension outside. The complex tensegrity balloon we see in Figure 10(a) can be derived from the seed structure shown in Figure 10(b) [10]. It is worth observing that by sectioning such a system, it is possible to obtain a shelter structure to be anchored to the ground, as shown in the model of Figure 10(c). This structure can also be transformed into a floating-bending system replacing struts with arches and adding a membrane. We observe that the nice MOOM installation realized by Kazuhiro Kojima and C+A in 2011 [11] can be regarded as a floating-bending system with straight beam elements.

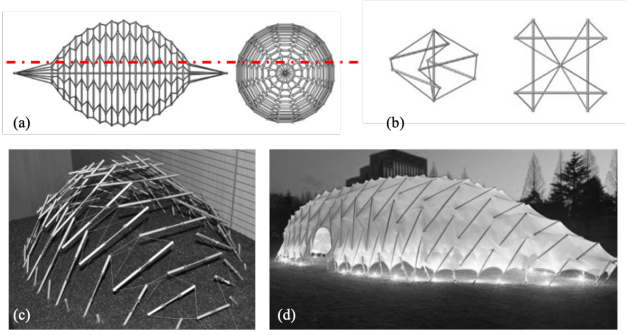

Figure 10: The tensegrity balloon in (a) can be obtained as a generalization of the seed structure in (b); (c) A section of the system in (a) can be isolated and anchored to the ground [10]; 80×60×40cm model realized by Davide Cadoni; (d) MOOM installation realized by Kazuhiro Kojima and C+A in 2011 [11].

Figure 11(a) shows another type of tensegrity balloon, one which was obtained by arranging struts in a weaving pattern inside a triangulated cable net [12]. It is also possible to consider balloons with openings (Figure 11b) and, similarly to the previous case, different anchored structures can be derived with sections (Figure 11c). A notable tensegrity membrane structure recalling these principles is the knitted tensegrity-membrane system presented at the Expo of the IASS 2019 Symposium in Barcelona [13]. It is further remarked that it is not yet clear whether it is possible or not to transform a tensegrity system, which does not belong to the diamond class, into a floating-bending structure.

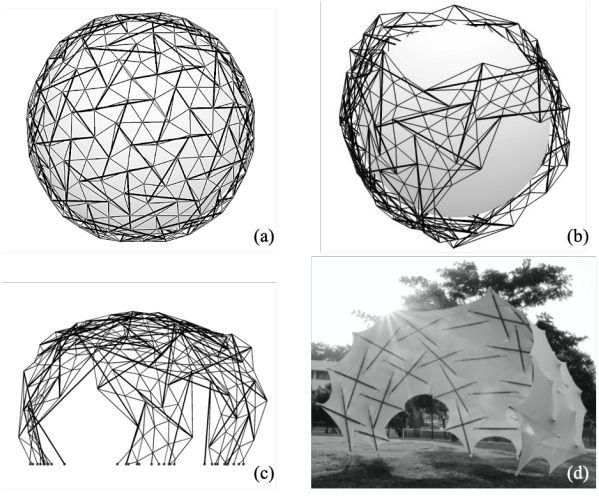

Figure 11: (a, b) Tensegrity balloons; (c) A section of the system in (b) constrained to ground; (d) Knitted tensegrity-membrane system presented at the Expo of the IASS 2019 Symposium in Barcelona [13]. Notice that in the top pictures a sphere is drawn inside the balloon for ease of visualization.

5 Concluding remarks

Floating-bending tensile-integrity structures can be regarded as continuous prestressed surfaces with "cable" and "arch" singularities. They can be derived from classical diamond-type tensegrity systems and can be exploited as deployable or transformable structures enclosing a larger space as compared to usual tensegrity systems, especially those with few struts. In this work, numerical form-finding and structural design calculations were performed for these types of structures for the first time, showing that floating-bending structures are feasible, and that they may provide interesting architectural and engineering solutions.

The two form-finding procedures employed here, the one combining the stick-and-spring and membrane elements, and the WinTess procedure, are quite different from each other. In the first case, the elastic energy was minimized in a large-displacement regime. In the second case, the Form-finding module of WinTess, based on the force-density method, was employed to obtain the equilibrium shape of membrane and cables, with arches fixed in space. Subsequently, the Analysis module of WinTess, based on the finite-element method, was employed to find the prestressed equilibrium configuration under self-weight, with arches free to move/deform. In this work, the first procedure constitutes a preliminary step to prove the feasibility of the floating-bending concept, while the second one provides a powerful tool for designing a floating-bending structure in a practical case of interest. We defer to a separate study the quantitative comparison between the performances of the two procedures.

Regarding future work, one of the first issues to be addressed is that of the existence of funicular arches, or the minimization of bending and torsion. Buckling and super-stability of this systems also need to be investigated. Furthermore, a trade-off analysis about structural efficiency and morphing capability, especially in comparison with traditional tensegrity system, is also called for in further investigations.

Acknowledgement: The authors wish to thank Prof. Ramon Sastre for providing the WinTess license, and together with Diana Peña for the suggestions on how to use the software. The authors also wish to thank Prof. Fernando Fraternali for some useful comments received during the preparation of this work. The contribution of Valentina Alleva who worked on her Master Thesis on this subject is gratefully acknowledged. Finally, the authors thank the anonymous reviewers for their suggestions which contributed to improve the quality of this paper.

Funding information: The authors state no funding involved.

Author contributions: All authors have accepted responsibility for the entire content of this manuscript and approved its submission.

Conflict of Interests: The authors state no conflict of interest.

References

[1] Sakantamis K, Popovic Larsen O. The cocoon method: a physical modelling tool for designing tensegrity systems. Int J Space Struct. 2004;19(1):11–20.

[2] Shigematsu M, Tanaka M, Noguchi H. Form finding analysis of tensegrity membrane structures based on variational method. In: Proceedings of IASS-IACM 2008 Spanning Nano to Mega (28-31 May 2008, Ithaca, New York, US). 2008

[3] Luchsinger RH, Pedretti M, Reinhard A. Pressure induced stability: from pneumatic structures to Tensairity. J Bionics Eng. 2004;1:141-148.

[4] Snelson K. The art of tensegrity. Int J Space Structures. 2012;27:71-80.

[5] Arcaro V. A simple procedure for shape finding and analysis of fabric structures. UNICAMP-FEC http://arcaro.org/tension/main.htm. 2004.

[6] Favata A, Micheletti A, Podio-Guidugli P, Pugno NM. Geometry and self-stress of single-wall carbon nanotubes and graphene via a discrete model based on a 2nd-generation REBO potential. J Elas. 2016;125:1–37.

[7] http://www.wintess.com

[8] Peña DM, Llorens I, Sastre R, Crespo D, Martinez J. Application of tensegrity to tensile-textile constructions: formfinding and structural analysis. In: Proceedings of IASS Symposium 2010 Spatial Structures – Permanent and Temporary (8-12 November 2010, Shanghai, China). 2010.

[9] Micheletti A, Tensegrity modules with orthogonal struts. In: Proceedings of IASS Symposium 2007 Architectural Engineering – Towards the Future Looking to the Past, (3-6 December 2007, Venice, Italy). 2007.

[10] Micheletti A, Cadoni D. Design of single-layer floating-compression tensegrities. In: Proceedings of 10^e Colloque National en Calcul des Structures (9-13 May 2011, Giens, France). 2011.

[11] Minimalistic Lightweight Construction: Temporary Pavilion in Noda. Detail. 2012;10:1086-8.

[12] Cadoni D, Micheletti A. Structural performances of single-layer tensegrity domes. Int J Space Struct. 2012;27(1-2):167-78.

[13] Gupta SS, Tan YY, Chia PZ, Pambudi CP, Yogiaman C, Tracy KJ. Knit tensegrity shell structures. In: Proceedings of IASS Symposium 2019 Form and Force (7-10 October 2019, Barcelona, Spain). 2019.